Performance Analysis of a 2D-MUSIC Algorithm for Parametric Near-Field Channel Estimation

Doğa Gürgünoğlu*, Alva Kosasih*, Parisa Ramezani*, Özlem Tuğfe Demir‡, Emil Björnson*, Gábor Fodor*†
*School of EECS, KTH Royal Institute of Technology, Stockholm, Sweden ({dogag,kosasih,parram,emilbjo,gaborf}@kth.se)
†Ericsson Research AB, Stockholm, Sweden ({doga.gurgunoglu,gabor.fodor}@ericsson.com)
‡Department of Electrical-Electronics Engineering, TOBB ETU, Ankara, Turkey (ozlemtugfedemir@etu.edu.tr)

***Abstract*—In this letter, we address parametric channel estimation in a multi-user multiple-input multiple-output system within the radiative near-field of the base station array with aperture antennas. We propose a two-dimensional multiple signal classification algorithm (2D-MUSIC) to estimate both the range and azimuth angles of arrival for the users' channels, utilizing parametric radiative near-field channel models. We analyze the performance of the proposed algorithm through the derivation of the Cramér-Rao lower bound (CRLB) for parametric estimation, and its effectiveness is compared against the least squares estimator, which is a non-parametric estimator. Numerical results indicate that the 2D-MUSIC algorithm outperforms the least squares estimator. Furthermore, the results demonstrate that the performance of 2D-MUSIC achieves the parametric channel estimation CRLB, which shows that the algorithm is asymptotically consistent.**

***Index Terms*—Radiative near-field, aperture antennas, MUSIC, channel estimation, Cramér-Rao lower bound.**

I. Introduction

The success of massive multiple-input multiple-output (M-MIMO) implementation in 5G systems, across both sub-6 GHz and mmWave bands, suggests that the next generation of wireless systems will likely exploit even larger arrays, referred to as the extremely large aperture array (ELAA) [1]–[3]. Moreover, there is an ongoing trend toward employing higher frequencies, implying a smaller wavelength in wireless systems [4], [5]. As the array size increases and the wavelength shrinks, the Fraunhofer array distance, the boundary between radiative near- and far-fields, becomes large. Consequently, the user equipments (UEs) are likely to fall into the radiative near-field region of the ELAA [6]. In the radiative near-field, the spherical curvature of the wavefront is noticeable; therefore, there are spherical phase variations between the antenna elements in the ELAA. The phase variations must be characterized by both the angle and distance between the ELAA and the transmitter. This renders far-field channel models inaccurate as the far-field array response does not capture information about the propagation distance.

To address this issue, polar-domain representation for the extremely large-scale MIMO (XL-MIMO) channel has been proposed in [7], [8]. Reference [7] focuses on the recovery of the angular and distance information in the near-field channel utilizing the sparsity in the polar domain, while [8] utilizes the distance domain in addition to the angular domain to multiplex UEs in line of sight (LOS) scenarios. With the polar-domain representation, one can sample both the angular and distance domains to obtain a near-field codebook. Moreover, the polar-domain representation is used to ensure a sparsity representation of the near-field channel, enabling the utilization of compressive sensing methods such as the classical orthogonal matching pursuit (OMP) and simultaneous iterative gridless weighted (SIGW) algorithms [7].

When the channel is pure-LOS, another way to estimate the near-field channel is to first estimate the parameters of the UEs' locations, given that the channel has a simple and known parametrization. Subsequently, the parameters are substituted into the channel parametric model to yield the channel estimate. A straightforward approach is to discretize the two-dimensional (2D) spatial domain and perform classical spectral estimation methods (e.g., multiple signal classification (MUSIC)) to estimate the location of the UEs in the 2D domain.

In this letter, we explore the possibility of estimating the UEs' locations in polar coordinates based on the 2D near-field channel model, where the channel is assumed to be pure-LOS. Then, we use the parameter estimates to infer the channel coefficients. In addition, we derive the Cramér-Rao lower bound (CRLB) on the parametric channel estimation mean squared error (MSE) to evaluate the performance of the 2D-MUSIC estimator. The CRLB provides a lower bound on the variance of any unbiased estimator [9], and depends heavily on the relationship between the observation and the parameter. Therefore, it is quite useful in evaluating parametric estimators. In [10], the CRLB on parametric channel estimation is derived with a far-field model for a system using two reconfigurable intelligent surfaces by considering the non-parametric CRLB as a transitional step towards a parametric channel estimation CRLB. To the best of the authors' knowledge, however, such an analysis has not been used to evaluate the performance of a parametric channel estimator. In this letter, we explore the opportunities of parametric channel estimation in near-field channels with aperture antennas by performing the aforementioned analysis. In addition to the CRLB analysis, we also compare the performance of the 2D-MUSIC algorithm with a non-parametric estimator, namely,

This study is supported by EU Horizon 2020 MSCA-ITN-METAWIRELESS, Grant Agreement 956256. This paper was supported by the Grant 2019-05068 from the Swedish Research Council.

the least squares (LS) estimator to observe the performance gain from parametric channel estimation.

II. System Model

We consider a base station (BS) equipped with a uniform linear array (ULA) consisting of N aperture antennas, serving K single-antenna UEs. The location of UE k is denoted as $(x_k, 0, z_k)$, which is assumed to be in the radiative near-field region (Fresnel region) of the BS array, for $k \in \{1, \ldots, K\}$. Without loss of generality, we let the BS be geometrically arranged along the x-axis with half-wavelength spacing, and the array is centered around $(0, 0, 0)$. Antenna element n is centered at $(\bar{x}_n, 0, 0)$ with

$$\bar{x}_n = \underbrace{\left(n - \frac{N+1}{2}\right)}_{\delta_n} \underbrace{\frac{\lambda}{2}}_{\Delta}, \tag{1}$$

where δ_n and Δ are the index of antenna element n and spacing between two antenna elements, respectively. The aperture antennas each have an area of Δ^2 along the xy-plane.

The channel between antenna element n and UE k located at the distance d_k (from the origin) in the azimuth angle φ_k with respect to the origin (measured from x-axis towards the z-axis) is represented as

$$h_n^k(d_k, \varphi_k) = \sqrt{\beta_{n,k}} e^{-\mathrm{j}\frac{2\pi}{\lambda} r_n^k}, \tag{2}$$

where $r_n^k = \sqrt{d_k^2 + (\delta_n \Delta)^2 - 2 d_k \Delta \delta_n \cos(\varphi_k)}$. The free-space channel gain between antenna n and UE k ($\beta_{n,k}$) can be approximated as

$$\beta_{n,k} \approx \beta_k = \frac{\lambda^2}{16\pi} \frac{\sin(\varphi_k)}{d_k^2} \tag{3}$$

which accounts for the effective antenna area as perceived by the transmitter, as well as the polarization loss. The approximation holds when the propagation distance is larger than twice the array aperture [6] so that the spherical amplitude variations over the wavefront are negligible but not the phase variations. Using (2) and (3), we can model the near-field channel vector to UE k as

$$\mathbf{h}_k(d_k, \varphi_k) = \sqrt{\beta_k} \left[e^{-\mathrm{j}\frac{2\pi}{\lambda} r_1^k} \ \ldots \ e^{-\mathrm{j}\frac{2\pi}{\lambda} r_N^k} \right]^{\mathrm{T}}. \tag{4}$$

At time instance l, the received signal can be written as

$$\mathbf{y}[l] = \mathbf{H}\mathbf{s}[l] + \mathbf{w}[l], \quad l = 1, \ldots, L, \tag{5}$$

where $\mathbf{H} = [\mathbf{h}_1(d_1, \varphi_1) \ \ldots \ \mathbf{h}_K(d_K, \varphi_K)]$, $\mathbf{y}[l] = [y_1[l] \ \ldots \ y_N[l]]^{\mathrm{T}}$ contains the received signals, $\mathbf{s}[l] = [s_1[l] \ \ldots \ s_K[l]]^{\mathrm{T}}$ represents the transmitted signals from K UEs, and $\mathbf{w}[l] = [w_1[l] \ \ldots \ w_N[l]]^{\mathrm{T}}$ is the additive noise where each entry follows an independent complex Gaussian distribution with zero mean and variance σ^2.

III. Near-Field Parametric Channel Estimation via 2D-MUSIC

In this section, our aim is to estimate the channels $\mathbf{h}_k(d_k, \varphi_k)$ for $k = 1, \ldots, K$ based on (5). Combining L such observations over time, we first aim to estimate the ranges d_k and azimuth angle of arrivals (AoAs) φ_k for $k = 1, \ldots, K$ using the 2D-MUSIC algorithm. The channel response function, defined in (2), allows us to characterize the UEs' channels by estimating the locations $(d_k, \varphi_k), k = 1, \ldots, K$, from L transmissions at distinct instants. This allows us to estimate the channels of the K UEs based on the d_k and φ_k by using the parametric model in (4). In the following, we provide a way to utilize 2D-MUSIC to estimate the UEs' channels. We assume that: 1) The UEs are not located in exactly the same angular directions. 2) The transmitted signals are assumed to follow a zero-mean complex Gaussian distribution. 3) The noise is independent of all the signals.

The MUSIC algorithm works by exploiting the structure of the eigenvectors in the sample covariance matrix:

$$\widehat{\mathbf{R}}_L = \frac{1}{L} \sum_{l=1}^{L} \mathbf{y}[l] \mathbf{y}^{\mathrm{H}}[l]. \tag{6}$$

Given the number of UEs K, we first construct the noise-subspace matrix $\widehat{\mathbf{U}}_{\mathrm{n}} \in \mathbb{C}^{N \times (N-K)}$ whose columns are the eigenvectors of $\widehat{\mathbf{R}}_L$ corresponding to the smallest $(N-K)$ eigenvalues. Then, the 2D MUSIC spectrum is generated as

$$S(d, \varphi) = \frac{1}{\mathbf{h}^{\mathrm{H}}(d, \varphi) \widehat{\mathbf{U}}_{\mathrm{n}} \widehat{\mathbf{U}}_{\mathrm{n}}^{\mathrm{H}} \mathbf{h}(d, \varphi)}, \tag{7}$$

where each possible value of $\mathbf{h}(d, \varphi)$ is obtained by computing the potential channel responses by plugging the grid points into (4). K combinations of (d, φ) corresponding to the peaks in the MUSIC spectrum are then identified, each representing a UE's location. The channel estimate $\widehat{\mathbf{H}}$ can then be obtained by substituting the parameter estimates $(d_k, \varphi_k), k = 1, \ldots, K$ into (2).

IV. CRLB on Near-Field Parametric Channel Estimation

In parameter estimation problems, bounds on estimation performance serve as the golden standard to evaluate the performance of estimators. To this end, we derive the CRLB on the near-field parametric channel estimation in this section. The CRLB, the inverse of the Fisher Information Matrix (FIM), provides a lower bound on the performance of any unbiased estimator [9] via the following matrix inequality:

$$\mathrm{Cov}\left(\hat{\boldsymbol{\theta}}(\mathbf{X})\right) \succeq \mathbf{I}^{-1}(\mathbf{X}; \boldsymbol{\theta}) \tag{8}$$

for an estimate of a parameter vector $\boldsymbol{\theta}$ based on an observation vector $\mathbf{X}$. Here, $\mathrm{Cov}(\hat{\boldsymbol{\theta}}(\mathbf{X})) = \mathbb{E}[(\hat{\boldsymbol{\theta}}(\mathbf{X}) - \boldsymbol{\theta})(\hat{\boldsymbol{\theta}}(\mathbf{X}) - \boldsymbol{\theta})^{\mathrm{H}}]$ is the covariance matrix and, consequently, the bound on the sum MSE can be expressed as

$$\mathbb{E}\left[\left\|\hat{\boldsymbol{\theta}}(\mathbf{X}) - \boldsymbol{\theta}\right\|^2\right] \geq \mathrm{tr}\left(\mathbf{I}^{-1}(\mathbf{X}; \boldsymbol{\theta})\right). \tag{9}$$

In a generic vector parameter estimation problem, the FIM is computed via the following equation [11, Eq. 3.21]:

$$[\mathbf{I}(\mathbf{X};\boldsymbol{\theta})]_{i,j} = -\mathbb{E}\left[\frac{\partial^2 \ln(f(\mathbf{X};\boldsymbol{\theta}))}{\partial\theta_i \partial\theta_j}\right], \tag{10}$$

where θ_i is the i-th element of $\boldsymbol{\theta}$. In our near-field parametric channel estimation problem, the observation from a single transmission is stated in (5). Before ensembling the observations from multiple transmissions, it is more convenient to change the order of the transmitted signals and the unknown channel in (5) as

$$\mathbf{y}[l] = \underbrace{\begin{bmatrix} s_1[l]\mathbf{I}_N & \dots & s_K[l]\mathbf{I}_N \end{bmatrix}}_{\triangleq \mathbf{S}[l] \in \mathbb{C}^{N \times NK}} \underbrace{\begin{bmatrix} \mathbf{h}_1(d_1,\varphi_1) \\ \vdots \\ \mathbf{h}_K(d_K,\varphi_K) \end{bmatrix}}_{\triangleq \tilde{\mathbf{H}}(\boldsymbol{\theta}) \in \mathbb{C}^{NK \times 1}} + \mathbf{w}[l], \tag{11}$$

where $\boldsymbol{\theta} \triangleq [d_1 \ \dots \ d_K \ \varphi_1 \ \dots \ \varphi_K]^{\mathrm{T}} \in \mathbb{R}^{2K}$. While (11) corresponds to the observation from a single transmission, we can stack the observations from multiple transmissions $l = 1, \dots, L$ vertically to obtain

$$\mathbf{Y} = \mathbf{S}\tilde{\mathbf{H}}(\boldsymbol{\theta}) + \mathbf{W} \in \mathbb{C}^{LN \times 1}, \tag{12}$$

where $\mathbf{Y} \triangleq [\mathbf{y}^{\mathrm{T}}[1] \ \dots \ \mathbf{y}^{\mathrm{T}}[L]]^{\mathrm{T}} \in \mathbb{C}^{LN}$, $\mathbf{S} \triangleq [\mathbf{S}^{\mathrm{T}}[1] \ \dots \ \mathbf{S}^{\mathrm{T}}[L]]^{\mathrm{T}} \in \mathbb{C}^{LN \times NK}$, and $\mathbf{W} \triangleq [\mathbf{w}^{\mathrm{T}}[1] \ \dots \ \mathbf{w}^{\mathrm{T}}[L]]^{\mathrm{T}} \in \mathbb{C}^{LN}$. To compute the FIM, we first define a transition parameter $\mathbf{V} \triangleq \tilde{\mathbf{H}}(\boldsymbol{\theta})$, for which we can express the FIM as

$$\mathbf{I}(\mathbf{Y};\mathbf{V}) = \mathbf{S}^{\mathrm{H}} \boldsymbol{\Sigma}_{\mathbf{W}}^{-1} \mathbf{S}, \tag{13}$$

where $\boldsymbol{\Sigma}_{\mathbf{W}} = \mathbb{E}[\mathbf{W}\mathbf{W}^{\mathrm{H}}] \in \mathbb{C}^{LN \times LN}$ is the noise covariance matrix, which has the following relationship with the noise covariance for a single transmission $\boldsymbol{\Sigma}_{\mathbf{w}} = \mathbb{E}[\mathbf{w}\mathbf{w}^{\mathrm{H}}] \in \mathbb{C}^{N \times N}$:

$$\boldsymbol{\Sigma}_{\mathbf{W}} = \mathbf{I}_L \otimes \boldsymbol{\Sigma}_{\mathbf{w}} = \sigma^2 \mathbf{I}_{LN}. \tag{14}$$

This relation holds since the noise is white over multiple transmissions.

A. CRLB for Vector Transformations

To incorporate the parametric nature of the channel into the CRLB analysis, we consider the parametric model $\tilde{\mathbf{H}}(\cdot) : \mathbb{R}^{2K} \mapsto \mathbb{C}^{NK}$ as a vector transformation to utilize the following identity [11, Eq. 3.30]:

$$\mathbf{I}^{-1}(\mathbf{Y};\mathbf{V}) = \mathbf{J}_{\tilde{\mathbf{H}}}^{\mathrm{H}} \mathbf{I}^{-1}(\mathbf{Y};\boldsymbol{\theta}) \mathbf{J}_{\tilde{\mathbf{H}}}, \tag{15}$$

where $\mathbf{J}_{\tilde{\mathbf{H}}} \in \mathbb{C}^{2K \times NK}$ is the Jacobian of the non-linear transformation $\tilde{\mathbf{H}} : \mathbb{R}^{2K} \mapsto \mathbb{C}^{NK}$ with entries $[\mathbf{J}_{\tilde{\mathbf{H}}}]_{i,j} = \frac{\partial \tilde{\mathbf{H}}_j}{\partial \theta_i}$. While (15) suffices to obtain the inverse FIM between the observation and the location parameters, the non-parametric FIM in (13) is not always invertible. Therefore, it is more desirable to have an expression for $\mathbf{I}(\mathbf{Y};\boldsymbol{\theta})$ in terms of $\mathbf{I}(\mathbf{Y};\mathbf{V})$. To this end, we multiply (15) with the pseudoinverse of $\mathbf{J}_{\tilde{\mathbf{H}}}$ from both sides to obtain

$$\mathbf{I}^{-1}(\mathbf{Y};\mathbf{V}) = \mathbf{J}_{\tilde{\mathbf{H}}}^{\mathrm{H}} \mathbf{I}^{-1}(\mathbf{Y};\boldsymbol{\theta}) \mathbf{J}_{\tilde{\mathbf{H}}} \Rightarrow \mathbf{J}_{\tilde{\mathbf{H}}} \mathbf{I}(\mathbf{Y};\mathbf{V}) \mathbf{J}_{\tilde{\mathbf{H}}}^{\mathrm{H}} = \mathbf{I}(\mathbf{Y};\boldsymbol{\theta}). \tag{16}$$

Combining (13) and (16) yields the $2K \times 2K$ FIM between the received signals and the UEs' coordinates. To obtain the parametric channel estimation CRLB, we invert $\mathbf{I}(\mathbf{Y};\boldsymbol{\theta})$ and apply (15):

$$\mathbf{I}^{-1}(\mathbf{Y};\tilde{\mathbf{H}}(\boldsymbol{\theta})) = \mathbf{J}_{\tilde{\mathbf{H}}}^{\mathrm{H}} \mathbf{I}^{-1}(\mathbf{Y};\boldsymbol{\theta}) \mathbf{J}_{\tilde{\mathbf{H}}}. \tag{17}$$

B. Jacobian of the Parametric Channel

To obtain the CRLB on the MSE of any parametric estimator for our setup, what remains is to derive the Jacobian of $\tilde{\mathbf{H}}(\cdot)$ in closed form. Based on the definition of $\tilde{\mathbf{H}}$ in (11), the Jacobian can be obtained as $\mathbf{J}_{\tilde{\mathbf{H}}} = [\mathbf{J}_1^{\mathrm{T}}, \mathbf{J}_2^{\mathrm{T}}]^{\mathrm{T}}$ where $\mathbf{J}_1, \mathbf{J}_2 \in \mathbb{C}^{K \times NK}$ are block diagonal matrices containing the partial derivatives of the channel with respect to d_k and φ_k, respectively. That is, $\mathbf{J}_1 = \operatorname{diag}\left(\frac{\partial \mathbf{h}_1^{\mathrm{T}}}{\partial d_1}, \dots, \frac{\partial \mathbf{h}_K^{\mathrm{T}}}{\partial d_K}\right)$ and $\mathbf{J}_2 = \operatorname{diag}\left(\frac{\partial \mathbf{h}_1^{\mathrm{T}}}{\partial \varphi_1}, \dots, \frac{\partial \mathbf{h}_K^{\mathrm{T}}}{\partial \varphi_K}\right)$. To derive $\frac{\partial \mathbf{h}_k}{\partial d_k}$ and $\frac{\partial \mathbf{h}_k}{\partial \varphi_k}$, we need to recall the near-field channel model parametrized by UE location in Section II. Starting from (4), we have

$$\begin{aligned} \frac{\partial \mathbf{h}_k}{\partial d_k} &= \frac{1}{2\sqrt{\beta_k}} \frac{\partial \beta_k}{\partial d_k} \begin{bmatrix} e^{-\mathrm{j}\frac{2\pi}{\lambda} r_1^k} & \dots & e^{-\mathrm{j}\frac{2\pi}{\lambda} r_N^k} \end{bmatrix}^{\mathrm{T}} \\ &+ \sqrt{\beta_k} \begin{bmatrix} -\mathrm{j}\frac{2\pi}{\lambda} \frac{\partial r_1^k}{\partial d_k} e^{-\mathrm{j}\frac{2\pi}{\lambda} r_1^k} & \dots & -\mathrm{j}\frac{2\pi}{\lambda} \frac{\partial r_N^k}{\partial d_k} e^{-\mathrm{j}\frac{2\pi}{\lambda} r_N^k} \end{bmatrix}^{\mathrm{T}}, \end{aligned} \tag{18a}$$

$$\begin{aligned} \frac{\partial \mathbf{h}_k}{\partial \varphi_k} &= \frac{1}{2\sqrt{\beta_k}} \frac{\partial \beta_k}{\partial \varphi_k} \begin{bmatrix} e^{-\mathrm{j}\frac{2\pi}{\lambda} r_1^k} & \dots & e^{-\mathrm{j}\frac{2\pi}{\lambda} r_N^k} \end{bmatrix}^{\mathrm{T}} \\ &+ \sqrt{\beta_k} \begin{bmatrix} -\mathrm{j}\frac{2\pi}{\lambda} \frac{\partial r_1^k}{\partial \varphi_k} e^{-\mathrm{j}\frac{2\pi}{\lambda} r_1^k} & \dots & -\mathrm{j}\frac{2\pi}{\lambda} \frac{\partial r_N^k}{\partial \varphi_k} e^{-\mathrm{j}\frac{2\pi}{\lambda} r_N^k} \end{bmatrix}^{\mathrm{T}}, \end{aligned} \tag{18b}$$

where $\frac{\partial \beta_k}{\partial d_k}$, $\frac{\partial \beta_k}{\partial \varphi_k}$, $\frac{\partial r_n^k}{\partial d_k}$ and $\frac{\partial r_n^k}{\partial \varphi_k}$ can be expressed as

$$\frac{\partial \beta_k}{\partial d_k} = -\frac{\lambda^2}{8\pi} \frac{\sin(\varphi_k)}{d_k^3}, \tag{19a}$$

$$\frac{\partial \beta_k}{\partial \varphi_k} = \frac{\lambda^2}{16\pi} \frac{\cos(\varphi_k)}{d_k^2}, \tag{19b}$$

$$\frac{\partial r_n^k}{\partial d_k} = \frac{d_k - \Delta\delta_n \cos(\varphi_k)}{\sqrt{d_k^2 + (\delta_n \Delta)^2 - 2 d_k \Delta \delta_n \cos(\varphi_k)}}, \tag{19c}$$

$$\frac{\partial r_n^k}{\partial \varphi_k} = \frac{d_k \Delta \delta_n \sin(\varphi_k)}{\sqrt{d_k^2 + (\delta_n \Delta)^2 - 2 d_k \Delta \delta_n \cos(\varphi_k)}}. \tag{19d}$$

As a result, we have $\mathbf{J}_{\tilde{\mathbf{H}}}$ and hence the CRLB for parametric channel estimation in closed form.

V. Numerical Results

In this section, we provide numerical examples to demonstrate the performance of the 2D-MUSIC algorithm. In addition, we include a non-parametric channel estimator, namely, the LS estimator. For both estimators, we use the CRLB as the benchmark. For the LS estimator, we use the non-parametric CRLB (inverse of (13)) and for 2D-MUSIC, we use the parametric CRLB we derived in Section IV. In addition, we examine the impact of the location of the UE on the channel estimation performance by considering a two-UE setup, assigning one of the UEs a fixed location, and changing the location of the other UE. We provide the parameters used to generate the numerical results in Table I.

TABLE I: List of parameters used to generate the numerical results.

Parameter	Value
N	32
L	40
K	4, 2[1]
SNR	$-10, -5, \ldots, 20$ dB
λ	10 cm

A. Performance of the 2D-MUSIC Algorithm

We first compare the estimation performance for the 2D-MUSIC algorithm and the LS estimator. As shown in Table I, we consider the signal-to-noise ratio (SNR) to be within the range of -10 dB and 20 dB. The UEs are dropped by selecting uniformly spaced points over the angular domain between $60\,\text{deg}$ and $120\,\text{deg}$, and between twice the aperture size and one-seventh of the Fraunhofer array distance to ensure radiating near-field conditions. In Fig. 1, we provide the CRLBs on the channel estimation normalized mean squared error (NMSE) for parametric and non-parametric estimators in blue and black solid lines, respectively. Then, we provide the NMSEs achieved by the 2D-MUSIC algorithm and the LS estimator with green and red lines.

Note that the LS estimator achieves the CRLB exactly as the number of observations is sufficient to estimate the channel. When considering the system model non-parametrically, the parameter undergoes a known linear transformation. Then, it is corrupted by additive Gaussian noise with known statistics. Therefore, the LS estimator achieves the CRLB exactly. On the other hand, the 2D-MUSIC algorithm performs significantly worse than the parametric CRLB at low SNR, where the algorithm performance is noise-limited. When the SNR is higher than $0\,\text{dB}$, however, the 2D-MUSIC algorithm performance achieves the parametric CRLB, showing that the MUSIC algorithm is asymptotically consistent. In addition, note that 2D-MUSIC consistently outperforms LS at all SNRs.

B. Location Dependence of the CRLB

In addition to the algorithm performance analysis, we also demonstrate how the parametric CRLB changes based on the UE location. To this end, we consider $K = 2$ UEs and fix the SNR to $10\,\text{dB}$. In addition, we fix the location of UE 1, denoted by the red dot in Fig. 2. Then, we compute the CRLB on the parametric channel estimation NMSE for UE 2 over a rectangular region, as shown in Fig. 2. While the antenna array is located at the origin, we choose our rectangular region so all the points are further than twice the aperture size and closer than the Fraunhofer distance to the antenna array.

Note that the CRLB increases as the UE moves towards the sides of the region and as the distance increases. On the other hand, the performance is not affected by UE 2's proximity to UE 1. This is because the system has enough observations and spatial degrees-of-freedom to accurately resolve the two UEs.

[1] $K = 2$ UEs are present in Fig. 2.

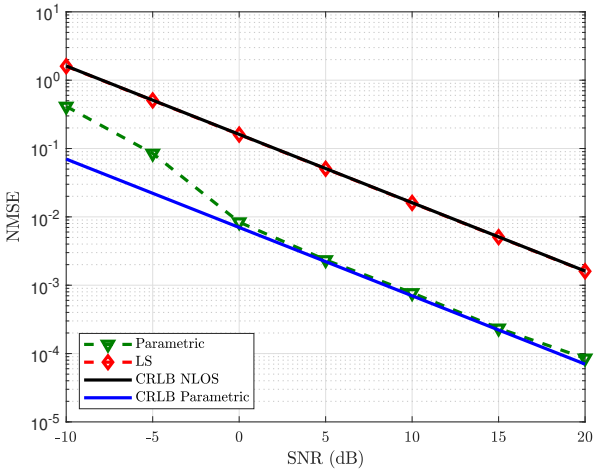

Fig. 1. SNR versus NMSEs of parametric and non-parametric channel estimation along with parametric and non-parametric CRLBs, for the parameters specified in Table I.

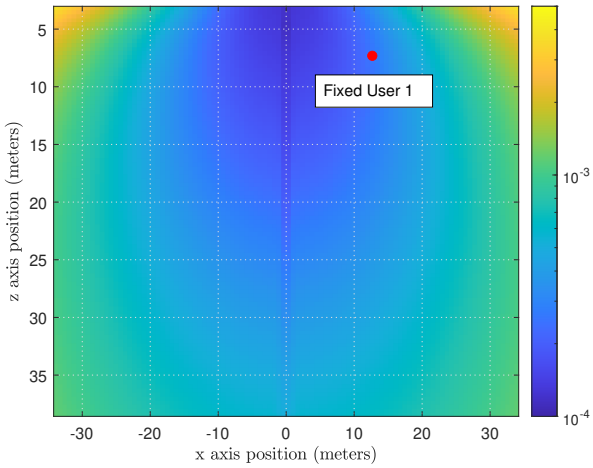

Fig. 2. CRLB of channel estimation for the second UE when the first UE's location is fixed. The SNR is fixed at $10\,\text{dB}$.

VI. Conclusions

In this letter, we considered the parametric channel estimation problem in a multiuser multiple-input multiple-output (MU-MIMO) setting where the UEs are within the radiative near field of the BS array. To this end, we proposed the use of the 2D-MUSIC algorithm, which estimates the range and azimuth AoAs of the UEs' channels, and obtains the channel estimates using the parametric near field channel models for aperture antennas. To evaluate the channel estimation performance of 2D-MUSIC, we derived the CRLB of parametric channel estimation in closed form and compared the 2D-MUSIC algorithm with a non-parametric estimator, namely the LS estimator. Our numerical results show that 2D-MUSIC outperforms the LS estimator, and it achieves the parametric channel estimation CRLB outside the noise-limited region. In addition, we also demonstrate that the 2D-MUSIC algorithm performance is close to the CRLB and hence is an efficient method to estimate the channel parametrically.

REFERENCES

[1] E. Björnson, L. Sanguinetti, H. Wymeersch, J. Hoydis, and T. L. Marzetta, "Massive MIMO is a reality—What is next? Five promising research directions for antenna arrays," *Digital Signal Processing*, vol. 94, pp. 3–20, Nov. 2019.

[2] H. Wang, A. Kosasih, C. -K. Wen, S. Jin and W. Hardjawana, "Expectation propagation detector for extra-large scale massive MIMO," *IEEE Trans. Wireless Commun.*, vol. 19, no. 3, pp. 2036–2051, Mar. 2020.

[3] A. Amiri, M. Angjelichinoski, E. de Carvalho, and R. W. Heath, "Extremely large aperture massive MIMO: Low complexity receiver architectures," in *Proc. IEEE Global Commun. Conf. Workshops*, UAE, Dec. 2018.

[4] T. S. Rappaport et al., "Wireless communications and applications above 100 GHz: Opportunities and challenges for 6G and beyond," *IEEE Access*, vol. 7, pp. 78 729–78 757, June 2019.

[5] L. Sanguinetti, E. Björnson, and J. Hoydis, "Toward massive MIMO 2.0: Understanding spatial correlation, interference suppression, and pilot contamination," *IEEE J. Sel. Areas Commun.*, vol. 68, no. 1, p. 232–257, Jan. 2020.

[6] E. Björnson and L. Sanguinetti, "Power scaling laws and near-field behaviors of massive MIMO and intelligent reflecting surfaces," *IEEE Open J. of the Commun. Soc.*, vol. 1, pp. 1306–1324, Sept. 2020.

[7] M. Cui and L. Dai, "Channel estimation for extremely large-scale MIMO: Far-field or near-field?" *IRE Trans. Commun.*, vol. 70, no. 4, pp. 2663–2677, Apr. 2022.

[8] Z. Wu and L. Dai, "Multiple access for near-field communications: SDMA or LDMA?" *IEEE J. Sel. Areas Commun.*, early access.

[9] H. V. Poor, *An Introduction to Signal Detection and Estimation (2nd Ed.)*. Berlin, Heidelberg: Springer-Verlag, 1994.

[10] D. Gürgünoğlu, E. Björnson, and G. Fodor, "Joint pilot-based localization and channel estimation in RIS-aided communication systems," *IEEE Wireless Communications Letters*, pp. 1–1, 2024.

[11] S. M. Kay, *Fundamentals of Statistical Signal Processing, Volume I: Estimation Theory*. Prentice Hall, 1993.